Vibrational Dynamics of Histamine Monocation in Solution: an Experimental (FT-IR, FT-Raman) and Theoretical (SCRF-DFT) Study

J. A. Collado,[†] I. Tuñón,[‡] E. Silla,[‡] and F. J. Ramírez*,[†]

Departamento de Química Física, Facultad de Ciencias, Universidad de Málaga, 29071-Málaga, and Departamento de Química Física, Universidad de Valencia, 46100-Burjassot (Valencia) Spain

Received: November 17, 1999

Structural and vibrational properties of histamine monocation in aqueous solution have been studied by means Fourier transform vibrational spectroscopies and a continuum model with the B3PW91 functional. Solvent effects were incorporated by means of an ellipsoidal cavity model with a multipolar expansion (up to six order) of the solute's electrostatic potential. Calculations were always performed at the 6-31+G* ab initio level. Solutions in water and deuterium oxide were investigated. Discussion was focused on the trans $N^{\tau}-H$ conformer of histamine monocation, which is the predominant structure in water solution. The optimized geometry was compared to that reported for this species in the solid state by diffraction techniques, where the only conformer present is the trans $N^{\tau}-H$. A general assignment was proposed for the infrared and Raman spectra of histamine monocation in solution, based on the isotopic shifts and a previous vibrational study in solid state. Force field and normal coordinate calculations were computed to support these assignments. The ab initio force constants were transformed into a set of locally symmetrized internal coordinates and subsequently scaled to the experimental frequencies by using one specific and two generic scaling factors. The comparison in terms of vibrational frequencies and normal coordinate descriptions supported most of the proposed assignments. The theoretical infrared spectra for the two isotopomers on the basis of the ab initio intensities also showed a good correlation with the experimental spectra. These results evidence that solute−solvent interactions must be explicitly taken into account in order to understand the vibrational behavior of polar species in solution; in addition, the use of multipolar expansions for the electrostatic potential together with a cavity adapted to the molecular shape improves significantly the performance of the solvation model.

Introduction

Histamine (2-aminoethyl-imidazole) is a biogenic amine present in a wide selection of living organisms, from unicellulars to superior animals,[1] which is synthesized from histidine.[2] Like other biogenic amines synthesized from amino acids (serotonine, tryptamine), histamine has some biochemical effects similar to those of the ornithine-derived polyamines (putrescine, spermidine, spermine). It is involved in several complex biological processes in which it interacts with specific receptors on the cell membranes.[3,4] Histamine stimulates many muscles to contract, which in some cases gives rise to vasodilation and a drop in blood pressure as a part of the body's defense mechanism.[5] The relations between histamine and allergies have been clearly established, as histamine is released when the body is invaded by external agents (drugs, proteins, etc.). Others physiological functions of histamine are related to stomach secretions, heart stimulation, inmunological reactions, etc.[3] Some synthetic polyamines, such as chlorfeniramine, also present such biochemical effects. Direct interactions between both biogenic and synthetic amines with nucleic acids have been proposed to explain some of their biological roles; these interactions lead to important structural changes in nucleic acids including twisting transitions, bending, triple helix stabilization, and condensation.[6−10]

Among the available techniques to study problems of molecular recognition, as the interaction between polyamines and nucleic acids, vibrational spectroscopy has some important advantages. The vibrational energy levels are very sensitive to structural modifications inside the molecules and to environmental changes. On the other hand, Raman spectroscopy allows for studying the biological systems in their natural medium, i.e., aqueous solutions, without sample damaging.[11−12] Fourier transform infrared and Raman spectroscopies have improved the performance of the vibrational studies by increasing factors as sensitivity, speed, resolution, etc.[13]

The usefulness of this experimental tool is nevertheless modulated by the knowledge of the vibrational spectra of the noninteracting systems, in the same physical environment. Thus, while the vibrational spectra of the nucleic acids have been widely studied,[14−17] this is not the case for histamine. Apart from an early article by Bellocq et al.,[18] the infrared and Raman spectra of this molecule have been scarcely revisited up to now.[19−20] In addition, we have not found in the literature any normal coordinate calculation to support the assignments based on experimental results. The aim of this work is therefore to present a thorough study of the vibrational dynamics of histamine in solution, at physiological pH, to propose a complete assignment of the infrared and Raman bands based on experimental (isotopic substitutions) and theoretical (high-level quantum chemical calculations) data. This study is a part of an extensive work aimed to analyze the interactions between natural and synthetic amines with the nucleic acids. As a first step, a vibrational analysis of solid histamine monohydrochloride and its N-deuterated isotopomer has been recently reported by our

* To whom correspondence should be addressed. E-mail: ramirez@uma.es.
[†] Universidad de Málaga.
[‡] Universidad de Valencia.

10.1021/jp994084d CCC: $19.00
Published on Web 02/23/2000

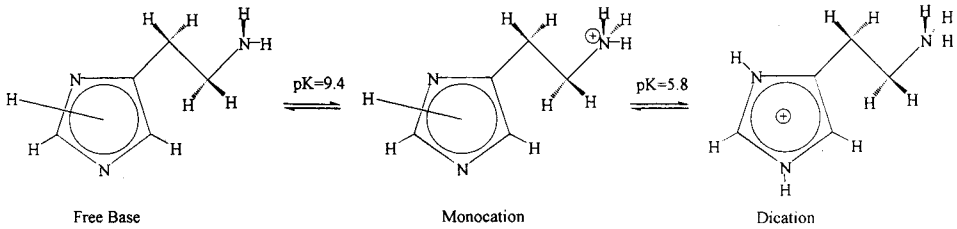

Figure 1. The three ionic species of the histamine molecule.

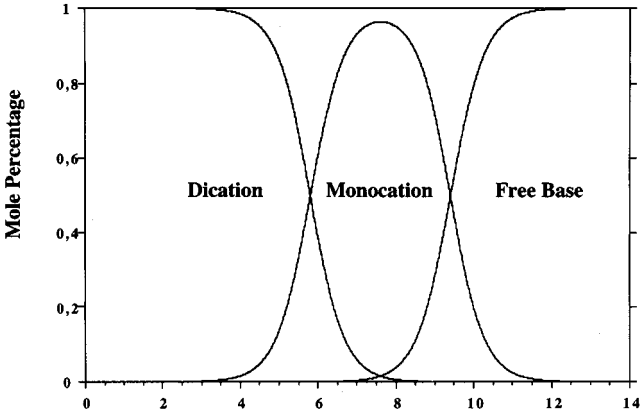

Figure 2. Molar ratios for the three ionic species of histamine molecule as a function of the pH.

laboratory.[21] These results will be of a great aid for comparing with the spectra of solved samples.

The theoretical treatment of polar species in solution has received an important amount of effort in the last few years.[22−23] On the other hand, there is a great variety of biological molecules which cannot be accurately studied without taking into account their interactions with the surroundings: zwitterions, cations or anions, strongly polar species, etc. Nowadays, the continuum solvent model has become one of the more popular methods of incorporating solvent effects into theoretical calculations of chemical systems.[24] Correlation energy seems to also play an important role.[25−26] Second-order Møller−Plesset perturbation theory (MP2) has been successfully used to describe the electronic repulsion; however, it originates a significant increment of the computational costs. An alternative methodology is the density functional theory (DFT),[27] which explicitly includes correlation energies with a moderate increasing of the calculation efforts. It has been shown[28] that scaled quantum mechanical (SQM) procedures in combination with ab initio−DFT force fields using moderate basis sets allow for a reliable prediction of the structural and vibrational properties of biomolecules. In the present paper, density functional theory and a continuum solvent model have been employed to study the vibrational dynamics of histamine in water solution, to give theoretical support to the experimental results.

Structurally, histamine free base is composed of an imidazole ring and an aminoethyl side chain. Both imidazole and aminoethyl moieties can accept a proton to give successively histamine monocation and dication, Figure 1. The pH of the medium and the two p*K*'s of histamine[29] determine therefore the ratios among these ionic species, as can be observed in Figure 2. At extreme basic pH histamine rejects its imidazole attached hydrogen giving the anion, while in a strongly acid pH we will have the dication. At physiological pH (around 7.4), the predominant species is the monocation (96%), hence this is the molecule in which we have focused our attention.

The present paper has been organized as follows. First, we give the experimental and computational methodology, and then the results are discussed in three sections, concerning: (i) the molecular structure and geometrical parameters, which were compared with some observed structures; (ii) the experimental infrared and Raman spectra of histamine in solution of H_2O and D_2O, giving a tentative assigment based on the isotopic shifts; (iii) a theoretical study of the vibrational dynamics, based on ab initio quantum mechanical calculations, in terms of frequencies, normal modes and quadratic force constants.

Experimental and Computational Methods

Histamine monohydrochloride was synthesized by mixing equimolecular amounts of histamine free base (supplied by Aldrich) and hydrogen chloride in solution, followed by evaporation in desiccator during several days. Deuteration was carried out as described elsewhere.[21] Aqueous solutions at a concentration 0.5 M were prepared by using alternatively tridistilled water and deuterium oxide (99.9 atom % D, Aldrich).

FT-IR and FT-Raman spectra were recorded at the room temperature in a Bruker EQUINOX 55 Fourier transform spectrometer, purged with dry nitrogen. FT-IR spectra were obtained placing the samples between calcium fluoride windows in a demountable cell for liquids, and using a potassium bromide beam splitter. FT-Raman spectra were obtained using excitation radiation at 1064 nm from a Nd:YAG laser working at 1w; the samples were placed in a mirrored quartz cuvette, and a calcium fluoride beam splitter was employed. A minimum of 500 scans were accumulated for all the spectra, at a resolution of 2 cm^{-1}.

Solute−solvent electrostatic interactions were simulated by employing the continuum model of Rivail et al.[30−32] In this model, the liquid is assimilated to a continuum characterized by a dielectric constant (78.4 for water). The quantum system is then placed in an ellipsoidal cavity whose volume is obtained by means of an empirical relation.[33] The electrostatic interaction is calculated using a multipolar moment expansion (up to sixth order) introduced in the Hamiltonian of the system. The analytical derivatives of this electrostatic term have been derived leading to an efficient geometry optimization procedure.[34] Geometry has been optimized using the redundant coordinates algorithm.[35] Cartesian force constants in solution have been calculated at the fully optimized geometry using analytical second derivatives.[36] All the calculations have been carried out using the hybrid functional B3PW91[37] and the 6-31+G* basis set.[38] This basis set, which includes polarization functions on all the atoms and diffuse functions on all the atoms except the hydrogens, has been suggested[39] as suitable to study vibrational features of strongly polar species in solution, and hence it has been selected for our calculations. Moreover, the hybrid functional B3PW91 has been successfully used to study the vibrational spectra of glycine and alanine amino acids in solution.[40] The GAUSSIAN package of programs[41] has been employed. For consideration of continuum solvent effects an extra link[42] has been added. Infrared absorption intensities were evaluated from the atomic polar tensors.[43]

The Cartesian force constants were transformed into a set of nonredundant locally symmetrized internal coordinates, defined

TABLE 1: B3PW91/SCRF/6-31+G* and Experimental[a] Structural Parameters for Histamine Monocation[b]

bond	calcd	exptl	angle	calcd	exptl	dihedral angle	calcd	exptl
N_1-C_2	1.357	1.349	$C_2-N_1-C_5$	107.8	108.4	$C_5-N_1-C_2-N_3$	−0.3	−2.1
N_1-C_5	1.373	1.362	$N_1-C_2-N_3$	111.2	110.0	$C_2-N_1-C_5-N_4$	−0.1	1.8
C_2-N_3	1.322	1.328	$C_2-N_3-C_4$	105.7	105.9	$N_1-C_2-N_3-C_4$	0.6	1.5
N_3-C_4	1.382	1.382	$N_1-C_5-C_4$	105.5	106.1	$C_2-N_3-C_4-C_5$	−0.6	−0.4
C_4-C_5	1.377	1.352	$N_3-C_4-C_5$	109.8	109.6	$N_1-C_5-C_4-N_3$	0.5	−0.8
N_1-H_6	1.014	0.94	$C_2-N_1-H_6$	126.6	109.7	$N_1-C_5-C_4-C_9$	−170.5	179.1
C_2-H_7	1.085	0.91	$N_1-C_2-H_7$	122.9	116.2	$N_3-C_4-C_9-C_{12}$	−74.6	−89.0
C_5-H_8	1.083	0.94	$N_1-C_5-H_8$	121.8	117.1	$C_4-C_9-C_{12}-N_{14}$	−178.7	177.3
C_4-C_9	1.504	1.498	$C_5-C_4-C_9$	128.0	128.8	$C_9-C_{12}-N_{14}-H_{16}$	176.5	−179.5
C_9-H_{10}	1.096	0.89	$C_4-C_9-H_{10}$	110.9	105.6	$C_9-C_{12}-N_{14}-H_{17}$	−62.9	−71.5
C_9-H_{11}	1.097	1.07	$C_4-C_9-H_{11}$	110.1	105.1	$C_9-C_{12}-N_{14}-H_{18}$	57.3	61.4
C_9-C_{12}	1.530	1.509	$C_4-C_9-C_{12}$	106.8	111.1			
$C_{12}-H_{13}$	1.088	0.97	$C_9-C_{12}-H_{13}$	110.5	118.2			
$C_{12}-H_{15}$	1.088	1.00	$C_9-C_{12}-H_{15}$	110.7	110.6			
$C_{12}-N_{14}$	1.504	1.505	$C_9-C_{12}-N_{14}$	115.5	110.6			
$N_{14}-H_{16}$	1.034	0.97	$C_{12}-N_{14}-H_{16}$	110.5	101.3			
$N_{14}-H_{17}$	1.024	0.83	$C_{12}-N_{14}-H_{17}$	111.9	107.3			
$N_{14}-H_{18}$	1.025	0.88	$C_{12}-N_{14}-H_{18}$	111.8	114.6			

[a] See Figure 3 for numbering. [b] Data correspond to solid histamine monohydrobromide.[53]

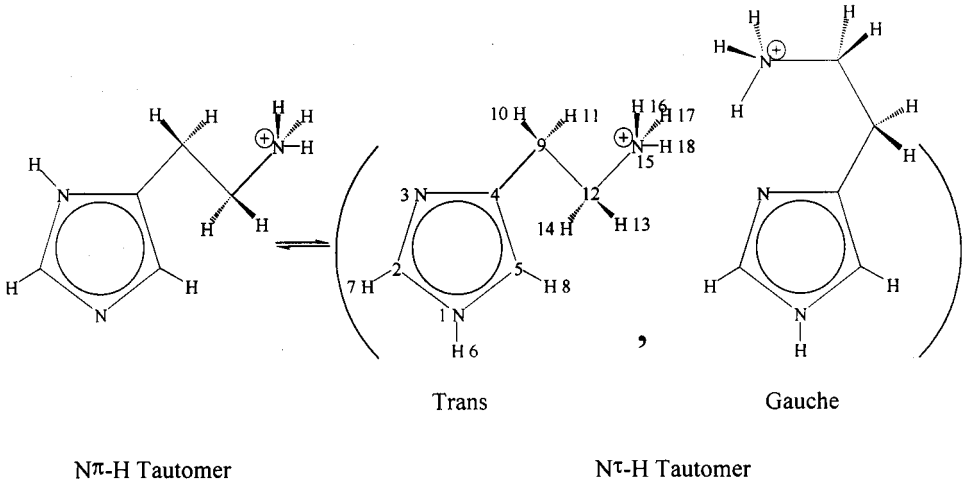

Figure 3. Tautomeric and conformational equilibria for histamine monocation. We have added the atomic numbering used in the calculations for the selected structure.

accordingly to the Pulay methodology.[44] This allows for a more useful description of the vibrational potential energy and make further calculations easier. The force field in internal coordinates was subsequently scaled, using a reduced number of factors calculated from the best experimental frequencies and assignments. Wavenumbers and normal coordinates were calculated by the Wilson FG matrix method.[45]

Results and Discussion

a. Structural Properties. The structure of histamine monocation has been the subject of several investigations to date. A first series of articles were published in the 1970's by Ganellin et al.[46−52] in which the structure of histamine and some derivatives were studied by theoretical and experimental procedures. Concerning the monocation (96% at physiological pH), they confirmed by potentiometric titration[46] that about 80% of the molecules in water solution are in the $N^{\tau}-H$ tautomer, which is also the only conformer existing in the solid state,[53] being the remainder 20% as the $N^{\pi}-H$ tautomer. In consequence, we have selected the more abundant tautomer for studying its vibrational properties. Both tautomers are able to undergo internal rotations to produce different conformers. Recently, some authors[54−57] have reported several theoretical structural studies about histamine species. An interesting result of these works indicates that the most stable structure of the isolated monocation is an imidazolium form in which two N−H bonds are located in the aromatic ring and an intramolecular hydrogen bond is present.[57] For the $N^{\tau}-H$ tautomer, two different conformers have been studied: (i) a gauche form which allows for an intramolecular hydrogen bond between the protonated nitrogen atom of the aminoethyl side chain and the proximal nitrogen atom of the imidazole ring and (ii) a trans form in which this interaction cannot be established. Evidently, in the gas phase, the gauche conformer is the prevaling form of the $N^{\tau}-H$ tautomer, being about 10−16 kcal/mol more stable, in internal energy, than the trans conformer.[57−58] However, in aqueous solution, experimental and theoretical evidence exists about the prevalence of the trans conformer.[58] In fact, it is believed that only about 20% of the $N^{\tau}-H$ tautomer exists in the gauche form in aqueous solution. The reason for the change in the energy order between the trans and gauche conformers of the $N^{\tau}-H$ tautomer when passing from the gas phase to the aqueous solution is the higher dipole moment of the former, and consequently, its larger solvation free energy.[58] The tautomeric equilibrium of histamine monocation and the conformational equilibrium of its $N^{\tau}-H$ tautomer are displayed in Figure 3.

Taking into account the aforementioned results, we have concentrated on the trans $N^{\tau}-H$ conformer of histamine monocation for the present vibrational study. As it is known, a

molecular geometry optimization is necessary before evaluating the energy derivatives. It was performed using the same computational methodology as for the force field calculation. The starting geometry was taken from that reported by Prout et al.[53] for histamine monohydrobromide from X-ray diffraction techniques, which coincides with the conformer selected for this study. As described elsewhere,[33] the axes of the ellipsoid are calculated after each optimization step from the new van der Waals volumes, being the final values $a = 2.656$ Å, $b = 3.105$ Å, and $c = 5.735$ Å. They preserve for a suitable interaction between the continuum polarizable medium and the molecular system inside the cavity. The optimized structural parameters (bond lengths and angles) are listed in Table 1, together with the starting parameters in order to compare them. From the comparison between both sets of data, some general trends can be pointed out. (i) Differences inside the imidazole ring are negligible; mean deviations are 0.01 Å for bonds lengths, 0.56° for bond angles, and 0.98° for dihedral angles. (ii) The structure of the ammonium group becomes regular as a consequence of the continuum polarizable medium around the cavity; in this case the deviations from the solid structure mainly affect to bond lengths and angles, being lower for the dihedrals. (iii) Small deviations are observed for the structural parameters of the side chain; however, significant differences existing for the methylene C−H bond lengths and angles in the crystal disappear in solution, as happens with the ammonium group. (iv) All the C−H and N−H distances increase from solid to solution, as a consequence of systematic overestimations; this fact will be also evident for the related vibrational frequencies, which will be corrected using a scaling procedure.

On the other hand, the Mulliken charge analysis indicates the electronic charge is far from being located exclusively on the ammonium group, or in the aliphatic side chain. The calculated net charge of the imidazole ring is +0.328, in electronic units, while the NH_3^+ group only remains +0.623 from the original +1.000 charge, it is to say, almost $^1/_3$ of the total charge is located on the imidazole ring, and $^2/_3$ on the side chain. We would like to emphasize that the calculated charge for the ring is close to that obtained for histamine free base using identical calculation methodology, +0.334.[59] This indicates that the electronic density into the imidazole ring for this species is almost identical than for the free base, despite their different molecular charge, and as a consequence properties directly dependent on the electronic density are expected to be similar. Thus, the intra-ring bond angles are calculated for both ionic species with a mean deviation of 0.002 Å, and a similar behavior is expected for related force constants and vibrational frequencies.

b. Infrared and Raman Spectra. The FT-IR and FT-Raman spectra of histamine monohydrochloride in solution of H_2O and D_2O are displayed in Figures 4 and 5, respectively. A general assignment of the measured bands, using a set of locally symmetrized vibrational modes defined elsewhere,[21] has been proposed on the basis of (i) the characteristic group frequencies, (ii) the isotopic shifts upon deuteration, (iii) reported vibrational data about this compound in the solid state,[21] and (iv) vibrational studies on related species in solution. Frequencies, relative intensities, and proposed assignments are listed in Tables 2 and 3 for natural histamine monocation and its N-deuterated derivative, respectively.

3500−2000 cm^{-1} Region. The analysis of the infrared spectra in this region is limited by the very strong and broad bands from the solvents. The spectrum of the D_2O solution also shows a residual H_2O band around 3400 cm^{-1}, due to quick hydrogen−deuterium interchanges during the sample manipulation and recording. The carbon−hydrogen stretching vibrations appear there as little shoulders, which can be enhanced by spectral subtraction, as displayed in Figure 5. The Raman technique improves the quality of the spectra in this region, because water molecules are bad scatters of radiation. Thus, the spectrum of histamine monohydrochloride in D_2O solution shows clear bands between 3200 and 2900 cm^{-1} which coincide with the infrared shoulders aforementioned. They can be also observed as shoulders of the solvent band in the Raman spectrum of the H_2O solution. In addition, some peaks at frequencies higher than 3200 cm^{-1} could belong to N−H stretching vibrations.

If we compare these frequencies with those reported for the C−H stretching vibration of solid histamine monocation,[21] some facts can be emphasize. Thus, while one imidazole ν(CH)

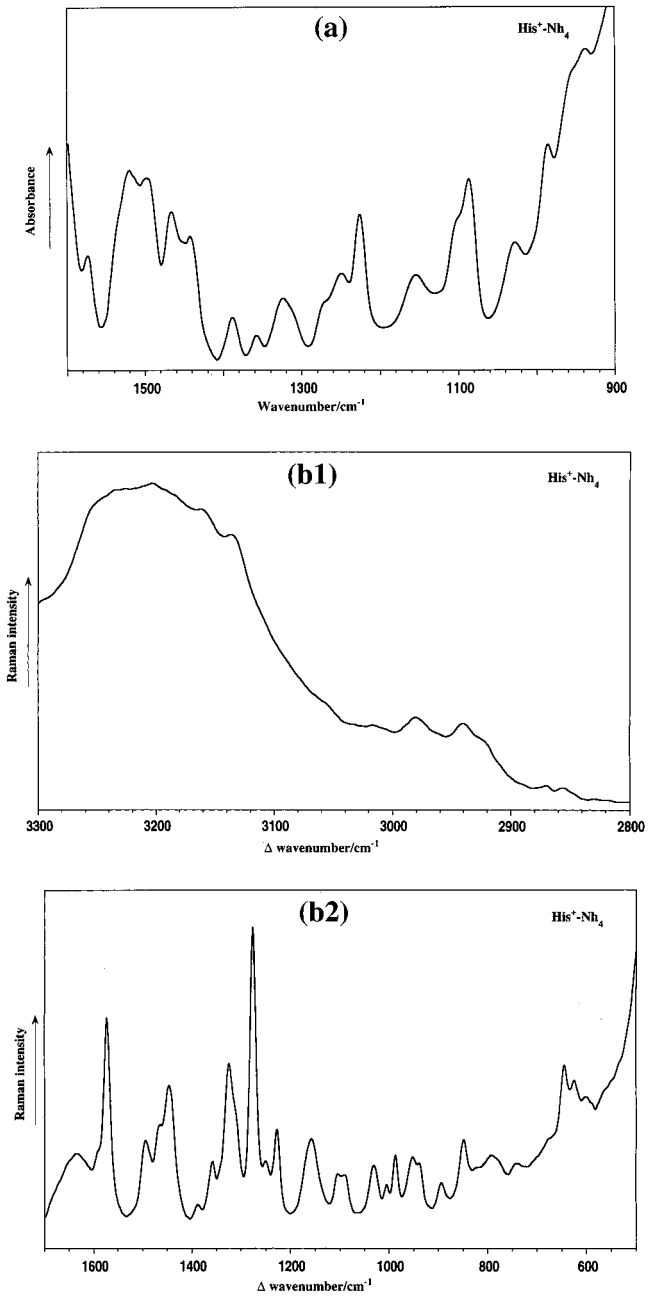

Figure 4. Fourier transform vibrational spectra of histamine monocation in H_2O solution: (a) infrared spectrum between 1600 and 900 cm^{-1}; (b1) Raman spectrum between 3300 and 2800 cm^{-1}; (b2) Raman spectrum between 1700 and 500 cm^{-1}.

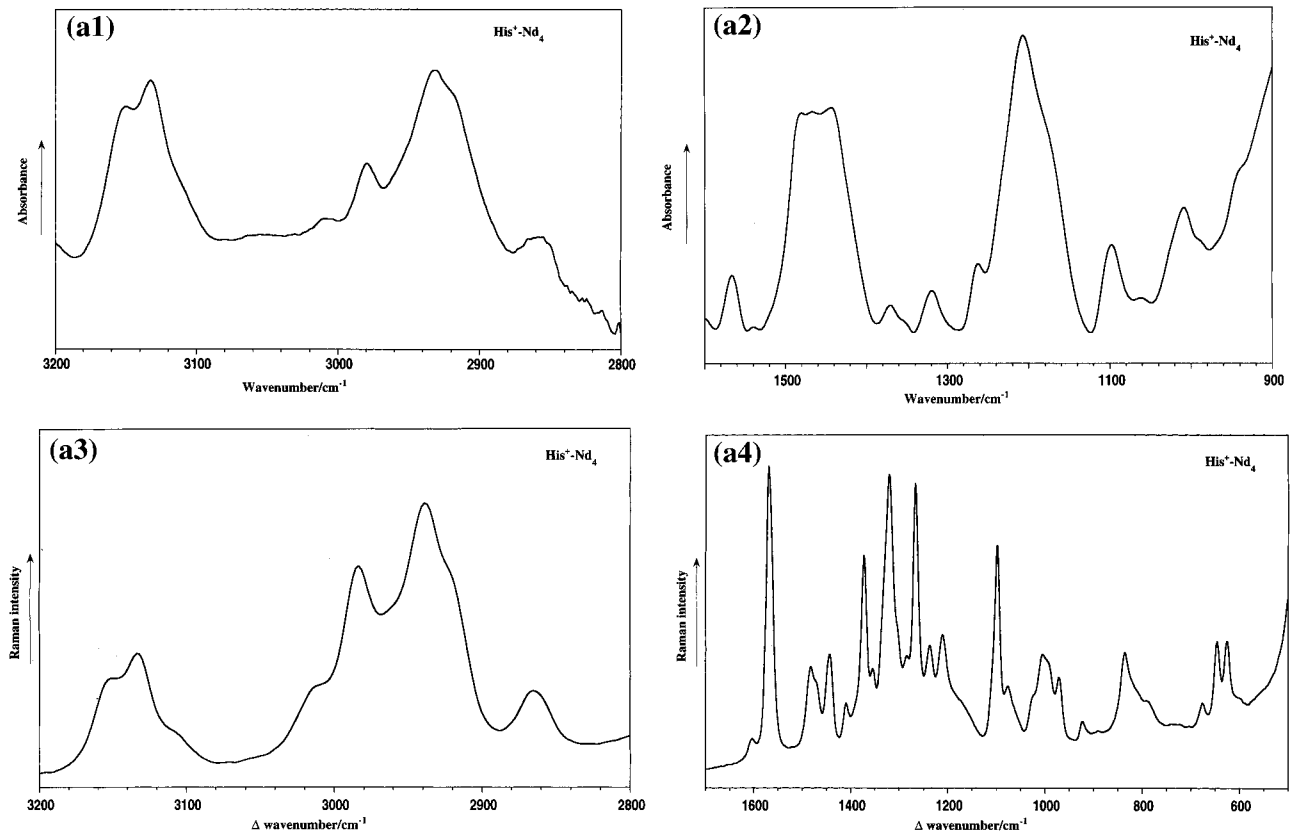

Figure 5. Fourier transform vibrational spectra of histamine monocation in D_2O solution: (a1) infrared spectrum between 3200 and 2800 cm^{-1}; (a2) infrared spectrum between 1600 and 900 cm^{-1}; (b1) Raman spectrum between 3200 and 2800 cm^{-1}; (b2) Raman spectrum between 1700 and 500 cm^{-1}.

frequency does not change from solid to solution, the other ν(CH) is observed with a difference of about 20 cm^{-1}. Significant deviations have been also evidenced for the methylene stretching modes. This behavior agrees with the differences observed for the C−H distances in the crystal,[53] which are expected to be closer in solution, as predicted by the calculations.

1600−500 cm^{-1} Region. The Raman spectrum of the H_2O solution shows an intense band at 1574 cm^{-1} that shifts by −6 cm^{-1} upon deuteration. This indicates small contributions from some N−H bending modes, which is expected for the imidazole ring stretching vibrations. Close to this band, a shoulder measured at 1591 cm^{-1} was not observed in the D_2O solution so that it has been assigned to an antisymmetrical ammonium bending vibration. They correlate well with the bands at 1602 and 1569 cm^{-1} of the Raman spectrum of solid histamine monocation assigned to identical vibrations.[21] In the infrared spectrum of the H_2O solution, the δ(OH) bending vibration only permits observation of the band at 1574 cm^{-1}, although a new absorption is observed at 1520 cm^{-1} that does not correlate with any frequency from the solid sample and disappears in the D_2O solution. Neighboring absorptions at 1498, 1467, and 1443 cm^{-1} have been confirmed in the Raman spectrum, appearing at 1483, 1470, and 1443 cm^{-1} upon deuteration, joint to a new band at 1410 cm^{-1}. The assignment of these frequencies to the local modes usually involved in this region seems to be troublesome. The band at 1443 cm^{-1} undoubtely corresponds to a $\delta(CH_2)$ bending vibration, and what appears at 1495 cm^{-1} clearly is an imidazole ring stretching mode. The second $\delta(CH_2)$ could correspond to the band at 1465 cm^{-1}; however, the Raman band at 1410 cm^{-1} evidences a vibration having nonvanished N−H contributions, which would lead to another ν(ring) stretching mode. In this case, this $\delta(CH_2)$ vibration is only observed in the spectra of D_2O solutions, and it would be hidden behind the intense imidazole stretching bands, both in the infrared and Raman spectra. As a consequence, the aforementioned band at 1520 cm^{-1} has to be assigned to the symmetrical bending mode of the ammonium group, $\delta_s(NH_3^+)$. Bellocq et al.[60] only measured the Raman bands at 1470 and 1454 cm^{-1}, proposing a mixed assignment for them, between $\delta(CH_2)$ and ν(ring). More recently, Davis et al.[61] registered the Raman spectrum of histamine monohydrochloride in aqueous solution, observing the bands at 1497 and 1450 cm^{-1}, while Itabashi et al.[62] measured the frequencies 1495 and 1450 cm^{-1}, adding some δ(NH) character to the first of them. No infrared data from histamine solutions have been reported up to now.

The comparison between the ammonium bending frequencies for solid and solved histamine monocation leads to interesting remarks. Thus, while the $\delta_a(NH_3^+)$ appears at near values, the $\delta_s(NH_3^+)$ for the solution shifts upward by 60 cm^{-1} with respect to the crystal.[53] The analysis of this fact in terms of intermolecular hydrogen bonds involving the ammonium group indicates that they have to be somewhat stronger in solution than in the solid state; however, changes in the related normal coordinates cannot be discarded. A second consequence is related to the conformation of this ionic species in solution. As previously discussed, a gauche structure that allows for an intramolecular hydrogen bond interaction exists, in addition to the predominant trans form. The vibrational frequencies from both solid and solution seem to indicate that this intramolecular interaction is rather relaxed by the solvation because no evidence of two different conformations has been found in the infrared and Raman spectra of the solutions.

In correlation with the measured and assigned frequencies for solid histamine monocation, several wagging and twisting

TABLE 2: Experimental Frequencies (in cm^{-1}) and Relative Intensities[a] Measured in the Infrared and Raman Spectra of Histamine−Nh_4 Molecule

infrared		Raman		
ν	I	$\Delta\nu$	I	assignments
		3202	sh	ammonium stretching
		3161	sh	imidazole C−H stretching
		3136	sh	imidazole C−H stretching
		3016	w	methylene stretching
		2981	m	methylene stretching
		2941	m	methylene stretching
		2930	sh	methylene stretching
		1591	sh	ammonium antisymmetric bending
1574	m	1574	s	imidazole ring stretching
1520	m			ammonium symmetric bending
1498	s	1495	m	imidazole ring stretching
1467	m−s	1465	m	imidazole ring stretching
1443	m	1446	m−s	methylene scissoring
1389	w−m	1388	w	methylene wagging
1358	w	1359	w−m	imidazole ring stretching
1324	w−m	1325	m−s	methylene twisting
1315	sh	1315	sh	methylene wagging
1272	sh	1276	vs	imidazole C−H in-plane bending
1249	m	1251	w−m	imidazole ring stretching
1226	m−s	1227	m	methylene twisting
1154	w−m	1158	m	ammonium rocking
1104	sh	1105	w−m	ammonium rocking
1087	s	1089	w−m	imidazole C−H in-plane bending
1028	m	1031	w−m	side-chain skeletal stretching
986	m	988	m	side-chain skeletal stretching
953	sh	953	w−m	imidazole N−H out-of-plane bend
938	w	939	sh	imidazole ring in-plane bending
		894	w	methylene rocking
		849	m	side-chain skeletal stretching
		794	w	imidazole C−H out-of-plane bend
		775	sh	imidazole C−H out-of-plane bend
		746	w	methylene rocking
		646	m	imidazole ring out-of-plane bending
		626	w−m	imidazole ring out-of-plane bending

[a] s = strong; m = medium; w = weak; v = very; sh = shoulder.

TABLE 3: Experimental Frequencies (in cm^{-1}) and Relative Intensities[a] Measured in the Infrared and Raman Spectra of Histamine-Nd_4 Molecule

infrared		Raman		
ν	I	$\Delta\nu$	I	assignments
3156	m	3149	m	imidazole C−H stretching
3139	s	3133	m−s	imidazole C−H stretching
3012	w−m	3010	m	methylene stretching
2981	m	2984	s	methylene stretching
2933	s	2938	vs	methylene stretching
2925	sh	2927	sh	methylene stretching
1567	m	1568	vs	imidazole ring stretching
1482	s	1483	m	imidazole ring stretching
1467	s	1470	sh	methylene scissoring
1443	s	1446	m	methylene scissoring
		1410	w	imidazole ring stretching
1371	w	1373	s	methylene wagging
1354	sh	1355	w	imidazole ring stretching
1319	w−m	1320	vs	methylene twisting
		1284	w	methylene wagging
1263	m	1267	vs	imidazole C−H in-plane bending
		1237	m	imidazole ring stretching
		1211	m	methylene twisting
		1190	sh	ammonium bending
1098	m	1098	s	ammonium bending
1061	w	1076	w	imidazole C−H in-plane bending
1009	m−s	1005	m	side-chain skeletal stretching
		971	w−m	side-chain skeletal stretching
		923	w	imidazole ring in-plane bending
		891	vw	methylene rocking
		837	m	ammonium rocking
		810	sh	side-chain skeletal stretching
		791	w	imidazole C−H out-of-plane bend
		741	vw	methylene rocking
		677	w	imidazole N−D out-of-plane bend
		646	m	imidazole ring out-of-plane bending
		626	m	imidazole ring out-of-plane bending

[a] s = strong; m = medium; w = weak; v = very; sh = shoulder.

modes have been assigned between 1400 and 1300 cm^{-1} for the solutions. In addition, a new imidazole ring stretching vibration at 1359 cm^{-1} has been proposed, which shifts downward by 4 cm^{-1} upon deuteration. The maximal shift observed for these bands was 15 cm^{-1}. A similar behavior occurs for the three bands observed between 1300 and 1200 cm^{-1} for the H_2O solution, namely at 1276, 1251, and 1227 cm^{-1} in the Raman spectrum. They have been assigned to δ(CH), ν(ring), and t(CH_2) vibrations, respectively, accordingly to their isotopic shifts. We would like to emphasize that no band from the spectra of the solutions can be well correlated with that measured at 1246 cm^{-1} for solid histamine monocation, which was assigned to the δ(NH) imidazole bending vibration. This means that the δ(NH) character should be widely distributed among the bands observed around 1250 cm^{-1}.

The two ammonium rocking vibrations have been assigned to the Raman bands at 1158 and 1105 cm^{-1} from the spectrum of the H_2O solution. They do not appear for the D_2O solution, thus supporting their assignments. Instead of them, a medium intensity band was measured at 1098 cm^{-1} which has been assigned to a $\delta(ND_3^+)$ vibration. These three frequencies have been also measured in the infrared spectra of the solution, namely at 1154, 1104, and 1098 cm^{-1}, respectively. The Raman spectrum of the D_2O solution also shows a broad shoulder at about 1190 cm^{-1} that could correspond to another $\delta(ND_3^+)$ bending vibration. It also appears as a shoulder of the strong infrared δ(OD) band originated by the solvent molecules.

Bands between 1100 and 900 cm^{-1} in the spectra of the H_2O solution have been assigned to side chain stretching and imidazole ring bending vibrations, with the exception of the band at 1089 cm^{-1}, that has been assigned to a δ(CH) bending mode, and that at 953 cm^{-1}, which is not observed when deuteration, being consequently assigned to the γ(NH) out-of-plane bending vibration. Shifts downward by about 20 cm^{-1} were observed for these bands, except for the γ(NH) mode, whose related N-deuterated vibration was assigned at 677 cm^{-1} in the Raman spectrum. The bands measured below 900 cm^{-1} have been assigned to the methylene rocking, imidazole out-of-plane and side-chain skeletal vibrations, taking into account the previous assignments proposed for solid histamine monocation. For molecules having a great number of degrees of freedom, as this case is, these vibrations are extensively coupled, and therefore to assign them to simple vibrational coordinates has to be considered as an approximate description.

c. Vibrational Dynamics. Second derivatives of the molecular energy in Cartesian coordinates were evaluated at the minimal energy geometry. These force constants were transformed into the set of nonredundant locally symmetrized internal coordinates listed in Table 4. This force field was improved by a scaling procedure in which the more consistent previous assignments were taken into account. However, and in order to preserve the essence of the calculational method, only two generic scaling factors have been used: 0.93 for the coordinates involving the hydrogen atoms and 0.96 for the coordinates involving only weight atoms (carbon and nitrogen). As an exception, a scaling factor of 0.90 was applied to the four methylene stretching vibrations, because they are very local

TABLE 4: Locally Symmetrized Internal Coordinates Used in This Work for Histamine Monocation

number	coordinate[a]	symbol	description
1	$r_{1,2}$	ν(ring)	ring stretch
2	$r_{2,3}$	ν(ring)	ring stretch
3	$r_{3,4}$	ν(ring)	ring stretch
4	$r_{4,5}$	ν(ring)	ring stretch
5	$r_{5,1}$	ν(ring)	ring stretch
6	$r_{1,6}$	ν(NH)	N−H stretch
7	$r_{2,7}$	ν(CH)	C−H stretch
8	$r_{5,8}$	ν(CH)	C−H stretch
9	$r_{4,9}$	ν(side chain)	side chain stretch
10	$r_{9,12}$	ν(side chain)	side chain stretch
11	$r_{12,15}$	ν(side chain)	side chain stretch
12	$2^{-1/2}(r_{9,10} + r_{9,11})$	$\nu_s(CH_2)$	CH_2 sym. stretch
13	$2^{-1/2}(r_{9,10} - r_{9,11})$	$\nu_a(CH_2)$	CH_2 antisym. stretch
14	$2^{-1/2}(r_{12,13} + r_{12,14})$	$\nu_s(CH_2)$	CH_2 sym. stretch
15	$2^{-1/2}(r_{12,13} + r_{12,14})$	$\nu_a(CH_2)$	CH_2 antisym. stretch
16	$3^{-1/2}(r_{15,16} + r_{15,17} + r_{15,18})$	$\nu_s(NH_3^+)$	NH_3^+ sym. stretch
17	$6^{-1/2}(2r_{15,16} - r_{15,17} - r_{15,18})$	$\nu_a(NH_3^+)$	NH_3^+ antisym. stretch
18	$2^{-1/2}(r_{15,17} - r_{15,18})$	$\nu_a(NH_3^+)$	NH_3^+ antisym. stretch
19	$0.632455\beta_{2,3,5} - 0.51167(\beta_{3,2,1} + \beta_{3,4,5}) + 0.195439(\beta_{2,1,5} + \beta_{1,5,4})$	δ(ring)	ring bend
20	$0.371748(\beta_{3,4,5} - \beta_{3,2,1}) + 0.601501(\beta_{2,1,5} - \beta_{1,5,4})$	δ(ring)	ring bend
21	$2^{-1/2}(\beta_{3,2,7} + \beta_{1,2,7})$	δ(CH)	CH in plane bend
22	$2^{-1/2}(\beta_{5,1,6} + \beta_{2,1,6})$	δ(NH)	NH in plane bend
23	$2^{-1/2}(\beta_{3,4,9} + \beta_{5,4,9})$	δ(CX)	ring in plane bend
24	$2^{-1/2}(\beta_{4,5,8} + \beta_{1,5,8})$	δ(CH)	CH in plane bend
25	$26^{-1/2}(5\beta_{10,9,11} + \beta_{5,9,12})$	$\delta(CH_2)$	CH_2 bend
26	$26^{-1/2}(5\beta_{5,9,12} + \beta_{10,9,11})$	δ(side chain)	side chain bend
27	$1/2(\beta_{12,9,10} + \beta_{12,9,11} - \beta_{5,9,10} - \beta_{5,9,11})$	$\omega(CH_2)$	CH_2 wagging
28	$1/2(\beta_{12,9,10} - \beta_{12,9,11} - \beta_{5,9,10} + \beta_{5,9,11})$	$t(CH_2)$	CH_2 twisting
29	$1/2(\beta_{12,9,10} - \beta_{12,9,11} + \beta_{5,9,10} - \beta_{5,9,11})$	$r(CH_2)$	CH_2 rocking
30	$26^{-1/2}(5\beta_{13,12,14} + \beta_{9,12,15})$	$\delta(CH_2)$	CH_2 bend
31	$26^{-1/2}(5\beta_{9,12,15} + \beta_{13,12,14})$	δ(side chain)	side chain bend
32	$1/2(\beta_{15,12,13} + \beta_{15,12,14} - \beta_{9,12,13} - \beta_{5,12,14})$	$\omega(CH_2)$	CH_2 wagging
33	$1/2(\beta_{15,12,13} - \beta_{15,12,14} - \beta_{9,12,13} + \beta_{5,12,14})$	$t(CH_2)$	CH_2 twisting
34	$1/2(\beta_{15,12,13} - \beta_{15,12,14} + \beta_{9,12,13} - \beta_{5,12,14})$	$r(CH_2)$	CH_2 rocking
35	$6^{-1/2}(\beta_{17,15,18} - \beta_{17,15,16} - \beta_{18,15,16} - \beta_{12,15,16} - \beta_{12,15,17} + \beta_{12,15,18})$	$\delta_s(NH_3^+)$	NH_3^+ sym. bend
36	$6^{-1/2}(2\beta_{17,15,18} - \beta_{17,15,16} - \beta_{18,15,16})$	$\delta_a(NH_3^+)$	NH_3^+ antisym. bend
37	$2^{-1/2}(\beta_{17,15,16} + \beta_{18,15,16})$	$\delta_a(NH_3^+)$	NH_3^+ antisym. bend
38	$6^{-1/2}(2\beta_{12,15,16} - \beta_{12,15,17} - \beta_{12,15,18})$	$r(NH_3^+)$	NH_3^+ rocking
39	$2^{-1/2}(\beta_{12,15,17} + \beta_{12,15,18})$	$r(NH_3^+)$	NH_3^+ rocking
40	ϕ_1	γ(NH)	NH out-pl bend
41	ϕ_2	γ(CH)	CH out-pl bend
42	ϕ_5	γ(CH)	CH out-pl bend
43	ϕ_4	γ(CX)	ring out-pl bend
44	$0.632455\tau_{3,5} - 0.51167(\tau_{3,2} + \tau_{4,5}) + 0.195439(\tau_{1,5} + \tau_{1,2})$	γ(ring)	ring out-pl bend
45	$0.371748(\tau_{4,5} - \tau_{3,2}) + 0.601501(\tau_{1,2} - \tau_{1,5})$	γ(ring)	ring out-pl bend
46	$\tau_{4,9}$	τ(side chain)	side chain torsion
47	$\tau_{9,12}$	τ(side chain)	side chain torsion
48	$\tau_{12,15}$	$\tau(NH_3^+)$	side chain torsion

[a] See Figure 3 for atomic numbering; $r_{i,j}$ is the stretching vibrations of the bond between atoms i and j; $\beta_{i,j,k}$ is the in-plane vibration of the angle between atoms i, j, and k; ϕ_i is the out-of-plane bending vibration of the atom i; τ_{ij} is the torsion vibration with respect to the bond between atoms i and j.

modes and can therefore be undoubtly assigned. The scaled frequencies and normal mode descriptions in terms of potential energy distribution (PED) are summarized in Tables 5 and 6 for the natural and N-deuterated derivative, respectively. Scaled diagonal force constants are listed in Table 7. Off-diagonal terms are available from the authors upon request.

The low-level scaling performed allows us to establish that the theoretical results are more the consequence of the calculational method than of the refinement process. In this way, and as a general trend, the calculated frequencies successfully adjust to the experimental ones, supporting the goodness of our methodology, while the normal mode descriptions confirm most of the proposed assignments for both H_2O and D_2O solutions of histamine monocation. We would like to point out that the agreement between calculated and observed data also exists for the isotopic shifts, which has, in our oppinion, great importance. As the most outstanding fact, the potential energy distribution does not assign the δ(NH) character to a single frequency but distributes it among several normal modes, as was predicted in the basis of the experimental isotopic shifts. In addition, the calculated frequency having the highest δ(NH) contribution, 1446 cm^{-1}, ν_{17}, falls down to 1381 cm^{-1} for the N-deuterated derivative, being the theoretical isotopic shift near to that experimentally measured. This downshift is not usual for deuterium substitution so that its successful prediction greately supports the physical model employed in the calculations. The normal coordinates associated with these frequencies are displayed in Figure 6 by the mean atomic displacement, together with a selection of other normal modes, to better visualize them.

The experimental frequencies between 2900 and 3200 cm^{-1} are correctly predicted. They are all very local modes, and a

TABLE 5: Scaled[a] B3PW91/SCRF/6-31+G* and Experimental Frequencies (cm^{-1}) for Histamine

vibration[b]	calcd	exptl	PED (greater than 10%)[c]
ν_1	3487		99 ν(NH)
ν_2	3401		99 $\nu_a(NH_3^+)$
ν_3	3352		64 $\nu_a(NH_3^+)$ + 32 $\nu_s(NH_3^+)$
ν_4	3222		68 $\nu_s(NH_3^+)$ + 36 $\nu_a(NH_3^+)$
ν_5	3159	3155	99 ν(CH)
ν_6	3142	3132	99 ν(CH)
ν_7	3060	3015	99 $\nu_a(CH_2)$
ν_8	2997	2985	100 $\nu_s(CH_2)$
ν_9	2957	2939	100 $\nu_a(CH_2)$
ν_{10}	2909	2918	100 $\nu_s(CH_2)$
ν_{11}	1633		90 $\delta_a(NH_3^+)$
ν_{12}	1619	1591	94 $\delta_a(NH_3^+)$
ν_{13}	1568	1574	66 ν(ring) + 14 ν(side chain) + 12 δ(CH)
ν_{14}	1516	1520	100 $\delta_s(NH_3^+)$
ν_{15}	1497	1495	67 ν(ring) + 33 δ(CH)
ν_{16}	1464	1467	99 $\delta(CH_2)$
ν_{17}	1446	1465	57 ν(ring) + 31 δ(NH) + 12 δ(ring)
ν_{18}	1437	1446	99 $\delta(CH_2)$
ν_{19}	1385	1388	89 $\omega(CH_2)$ + 14 ν(side chain)
ν_{20}	1345	1359	77 ν(ring) + 16 $t(CH_2)$
ν_{21}	1333	1325	66 $t(CH_2)$ + 10 $r(NH_3^+)$
ν_{22}	1317	1315	51 $\omega(CH_2)$ + 24 ν(ring) + 21 ν(side chain)
ν_{23}	1270	1276	32 $\omega(CH_2)$ + 17 $t(CH_2)$ + 11 δ(CH)
ν_{24}	1248	1251	29 ν(ring) + 22 $t(CH_2)$
ν_{25}	1216	1227	53 δ(CH) + 14 $r(CH_2)$
ν_{26}	1125	1158	24 ν(ring) + 18 $r(NH_3^+)$ + 14 ν(side chain) + 15 δ(NH)
ν_{27}	1118	1105	23 ν(ring) + 20 $r(NH_3^+)$ + 16 ν(side chain) + 15 δ(NH)
ν_{28}	1080	1087	39 ν(ring) + 33 δ(CH)
ν_{29}	1051	1031	49 $t(CH_2)$ + 21 $r(NH_3^+)$
ν_{30}	1000	988	85 ν(side chain) + 13 $r(NH_3^+)$
ν_{31}	964	953	44 δ(ring) + 31 ν(ring) + 10 ν(side chain)
ν_{32}	922	939	82 δ(ring)
ν_{33}	908	894	41 $r(NH_3^+)$ + 37 $r(CH_2)$
ν_{34}	899	849	45 ν(side chain) + 32 $r(NH_3^+)$
ν_{35}	814	794	65 γ(CH) + 34 γ(ring)
ν_{36}	766	775	79 γ(CH) + 20 γ(ring)
ν_{37}	741	746	95 $r(CH_2)$
ν_{38}	723		27 γ(ring) + 16 γ(CH) + 11 γ(CX) + 19 ν(side chain)
ν_{39}	685		27 γ(ring) + 16 ν(side chain) + 14 γ(CX) + 20 δ(side chain)
ν_{40}	654	646	86 γ(ring) + 14 γ(NH)
ν_{41}	575	626	89 γ(NH) + 11 γ(ring)
ν_{42}	368	384	26 γ(ring) + 24 δ(side chain)
ν_{43}	333		70 δ(CX)
ν_{44}	308		71 δ(side chain) + 12 γ(CX) + 11 γ(ring)
ν_{45}	239		100 $\tau(NH_3^+)$
ν_{46}	107		53 δ(side chain) + 32 γ(CX) + 15 γ(ring)
ν_{47}	92		62 τ(side chain) + 14 γ(CX)
ν_{48}	62		100 τ(side chain)

[a] Scaled factors were applied to the force constants. [b] Arbitrary numbering. [c] The symbols correspond to the coordinates listed in Table 4. Coordinates with similar characters were added to clarify.

TABLE 6: Scaled[a] B3PW91/SCRF/6-31+G* and Experimental Frequencies (cm^{-1}) for Histamine Monocation-d_4

vibration[b]	calcd	exptl	PED (greater than 10%)[c]
ν_1	3159	3156	99 ν(CH)
ν_2	3142	3133	99 ν(CH)
ν_3	3060	3012	99 $\nu_a(CH_2)$
ν_4	2997	2984	100 $\nu_s(CH_2)$
ν_5	2957	2938	100 $\nu_a(CH_2)$
ν_6	2909	2927	100 $\nu_s(CH_2)$
ν_7	2566		98 ν(ND)
ν_8	2510		100 $\nu_a(ND_3^+)$
ν_9	2460		86 $\nu_a(ND_3^+)$ + 11 $\nu_s(ND_3^+)$
ν_{10}	2326		87 $\nu_s(ND_3^+)$ + 13 $\nu_a(ND_3^+)$
ν_{11}	1562	1568	69 ν(ring) + 19 ν(side chain) + 12 δ(CH)
ν_{12}	1489	1483	77 ν(ring) + 35 δ(CH)
ν_{13}	1464	1467	96 $\delta(CH_2)$
ν_{14}	1437	1446	99 $\delta(CH_2)$
ν_{15}	1381	1410	68 ν(ring) + 19 $\omega(CH_2)$ + 14 δ(ND) + 10 δ(ring)
ν_{16}	1378	1373	77 $\omega(CH_2)$ + 24 ν(ring)
ν_{17}	1341	1355	77 ν(ring) + 15 $t(CH_2)$
ν_{18}	1311	1320	62 $t(CH_2)$
ν_{19}	1307	1284	56 $\omega(CH_2)$ + 15 ν(side chain)
ν_{20}	1261	1263	37 $\omega(CH_2)$ + 35 ν(ring) + 12 δ(CH)
ν_{21}	1232	1237	28 $t(CH_2)$ + 28 δ(CH) + 18 ν(ring)
ν_{22}	1200	1211	48 δ(CH) + 19 $r(CH_2)$ + 11 $t(CH_2)$
ν_{23}	1180	1190	51 $\delta_a(ND_3^+)$ + 40 $\delta_s(ND_3^+)$
ν_{24}	1164		97 $\delta_a(ND_3^+)$
ν_{25}	1162	1098	53 $\delta_s(ND_3^+)$ + 41 $\delta_a(ND_3^+)$
ν_{26}	1086	1076	47 ν(ring) + 24 δ(CH)
ν_{27}	1067		64 ν(side chain)
ν_{28}	1028	1005	42 $r(CH_2)$ + 26 $t(CH_2)$ + 15 ν(ring)
ν_{29}	984	971	35 ν(ring) + 31 δ(ring)
ν_{30}	933	923	61 ν(side chain)
ν_{31}	908	891	76 δ(ring)
ν_{32}	840	837	71 δ(ND) + 14 δ(ring)
ν_{33}	814	810	67 γ(CH) + 33 γ(ring)
ν_{34}	788	791	55 $r(CH_2)$ + 28 $r(ND_3^+)$ + 18 $t(CH_2)$
ν_{35}	767		51 γ(CH) + 34 $r(ND_3^+)$
ν_{36}	759	741	56 γ(CH) + 22 $r(ND_3^+)$ + 21 ν(side chain)
ν_{37}	716		31 γ(ring) + 17 γ(CX) + 12 γ(CH)
ν_{38}	692	677	51 $r(ND_3^+)$ + 49 $r(CH_2)$
ν_{39}	670	646	22 δ(ring) + 17 γ(ring) + 20 ν(side chain) + 11 $r(ND_3^+)$
ν_{40}	617	626	43 γ(ring) + 12 γ(ND)
ν_{41}	459		62 γ(ND) + 38 γ(ring)
ν_{42}	358		31 γ(ring) + 23 δ(side chain) + 13 δ(CX)
ν_{43}	320		67 δ(CX)
ν_{44}	280		70 δ(side chain) + 10 γ(CX)
ν_{45}	176		100 $\tau(ND_3^+)$
ν_{46}	103		62 δ(side chain) + 35 γ(CX) + 20 γ(ring)
ν_{47}	88		63 τ(side chain) + 17 γ(CX) + 17 δ(ring) + 12 γ(ring)
ν_{48}	58		100 τ(side chain)

[a] Scaled factors were applied to the force constants. [b] Arbitrary numbering. [c] The symbols correspond to the coordinates listed in Table 4. Coordinates with similar characters were added to clarify.

good fitting between calculated and experimental data can be easily reached. Concerning the $\delta(NH_3^+)$ vibrations, the bands measured at 1591 and 1520 cm^{-1} have been calculated at 1619 and 1516 cm^{-1}, respectively. The experimental frequency of 1520 cm^{-1} was significantly far from that proposed for solid histamine monocation, namely 1460 cm^{-1},[21] and its close theroretical prediction is a new relevant test for the goodness of the present calculation.

Imidazole ring stretching vibrations assigned at 1574, 1495, 1465, 1359, and 1251 cm^{-1} for the natural derivative were successfully estimated at 1568, 1497, 1446, 1345, and 1248 cm^{-1}, respectively. We would like to emphasize the agreement also achieved for the experimental and calculated isotopic shifts, namely 7(6), 13(8), 55(65), 5(4), and 14(16) cm^{-1}, with the values in parentheses being the theoretical results. As it is displayed in Figure 6, the related normal modes are rather similar for the two isotopomers. Concerning side chain vibrations, the infrared and Raman spectra of the solutions showed nonvanished isotopic shifts, about 10−15 cm^{-1}, for several methylene bending and skeletal stretching vibrations between 1400 and 1000 cm^{-1}, which indicate some vibrational contributions involving the acidic hydrogens. They have been confirmed by the theoretical results, and largely arise from the δ(NH) and $r(NH_3^+)$ coordinates.

The calculated frequencies and descriptions below 1000 cm^{-1} also show the general trends. However, the following results lead us to modify the proposed experimental assignments. (i) The Raman frequencies 988 and 939 cm^{-1} were assigned to

TABLE 7: SCRF Scaled Diagonal Force Constants (mdyn/Å or Equivalent Unit) Obtained for Histamine Monocation in an Ellipsoidal Cavity

coord[a]	symbol	force const.	coord[a]	symbol	force const.
1	ν (ring)	6.97	25	δ (CH_2)	0.77
2	ν (ring)	8.10	26	δ (side chain)	1.21
3	ν (ring)	5.90	27	ω (CH_2)	0.66
4	ν (ring)	7.45	28	t (CH_2)	0.65
5	ν (ring)	6.67	29	r (CH_2)	0.71
6	ν(NH)	6.72	30	δ (CH_2)	0.78
7	ν(CH)	5.38	31	δ (side chain)	1.12
8	ν(CH)	5.43	32	ω (CH_2)	0.70
9	ν(side chain)	4.66	33	t (CH_2)	0.68
10	ν(side chain)	4.17	34	r (CH_2)	0.86
11	ν(side chain)	4.10	35	δ_s (NH_3^+)	0.59
12	ν(side chain)	4.77	36	δ_a (NH_3^+)	0.61
13	ν_a (CH_2)	4.71	37	δ_a (NH_3^+)	0.62
14	ν_s (CH_2)	5.06	38	r (NH_3^+)	0.67
15	ν_a (CH_2)	5.02	39	r (NH_3^+)	0.64
16	ν_s (NH_3^+)	6.18	40	γ (NH)	0.18
17	ν_a (NH_3^+)	5.94	41	γ (CH)	0.35
18	ν_a (NH_3^+)	6.29	42	γ (CH)	0.36
19	δ (ring)	1.73	43	γ (CX)	0.43
20	δ (ring)	1.81	44	γ (ring)	0.47
21	δ (CH)	0.50	45	γ (ring)	0.53
22	δ (NH)	0.45	46	τ (side chain)	0.10
23	δ (CX)	0.67	47	τ (side chain)	0.09
24	δ (CH)	0.44	48	τ (NH_3^+)	0.09

[a] See Table 4 for coordinate descriptions.

ν(side chain) and δ(ring) vibrations, respectively, and have been undoubtly confirmed by the calculations, as can be seen in Table 5; their respective frequencies for the N-deuterated species were measured at 971 and 923 cm^{-1}, being assigned to the same vibrations, Table 3. The normal coordinate analysis correlates these bands with the frequencies 984 and 933 cm^{-1}, Table 6, although their descriptions are permuted at the light of the potential energy distribution. (ii) The imidazole out-of-plane N−H vibration was assigned to the band at 953 cm^{-1}, because it was not observed when deuteration; the nearest frequency of the theoretical spectrum is 964 cm^{-1}, but it is described as an imidazole skeletal mode while the γ(NH) vibration is calculated at 575 cm^{-1}. The true assignment of that band remains, therefore, uncertain. In our opinion, it could be related to the ammonium rocking vibrations. (iii) The vibrations r(ND_3^+) and γ(ND) were assigned to the observed bands at 837 and 677 cm^{-1}, respectively; they have been calculated at 840 and 692 cm^{-1}, but their characters are mainly δ(ND) and r(ND_3^+), respectively, as can be observed in the Figure 6. Because they all involve the acidic hydrogens, their assignments can be modified accordingly with the calculations.

The diagonal force constants are listed in Table 7. Concerning the imidazole ring stretching coordinates, their values clearly indicate the position of the two double bonds, in a localized bond description. Moreover, they are also influenced by the N1 position, which participates in the π-system with two electrons, while the rest of the atoms give one each. Thus, these force constants decrease following the series $f_{2,3} > f_{4,5} > f_{1,2} > f_{5,1} > f_{3,4}$, from 8.10 to 5.90 mdyn/Å. We can compare these values with those reported for solid imidazole from a refined force field based on inelastic neutron scattering experiments at 20 K;[63] in this state, an intermolecular N−H···N hydrogen bond is present. We can observe that while all the ring stretching force constants are somewhat greater, the ordering is not altered. Indeed, force constants for bonds involving the N atom having the lone pair (N3) show less deviations than the rest. This behavior can be explained from the different environments. In our theoretical model for the solvated molecule, the interaction with the solvent is stronger for the aforementioned N3 atom, which can justify the similar force constants for the neighboring bonds. Another outstanding consequence is the deviations existing for the X−H (X = N, C) stretching force constants; while the values for C−H bonds are close for both solid and solution, those of the N−H stretching deviate by about 2.5 mdyn/Å, namely 4.25 mdyn/Å (ref 63) and 6.72 mdyn/Å (present work).

All the side chain skeletal stretching force constants have similar values, showing some decreasing when going far from the cycle. Negligible differences have been calculated for coordinates having the same character, as a consequence of the continuum polar environment, and contrarily to what occurs in the solid. Concerning bending force constants, the higher values have been calculated for the imidazole ring, around 1.75 mdyn/Å, followed by the side chain skeletal, as expected. The rest of bending coordinates have force constants below 1 mdyn/Å, the three side chain torsional force constants being around 0.09 mdyn/Å. Negligible values for the off-diagonal force constants have been calculated.

Finally, we have displayed in Figures 7 and 8 the theoretical infrared spectrum of the natural and N-deuterated derivatives, respectively, for the spectral regions free from the strongest solvent absorptions. Pure ab initio intensities were used in combination with the scaled frequencies because they have not been greatly modified (in fact the frequency order has not be altered in any case). The comparison with the experimental infrared spectra can be considered satisfactory. The very strong band of the calculated spectrum for the natural derivative corresponds to the theoretical frequency of 1516 cm^{-1}, $\delta(NH_3^+)$, which has been correlated with the strong infrared absorption at 1520 cm^{-1}, thus supporting its assignment. The medium intensity infrared bands at 1498, 1443, 1226, and 986 cm^{-1} can be well correlated, in light of their intensities, to the theoretical bands at 1497, 1437, 1216, and 1000 cm^{-1}. Concerning the N-deuterated isotopomer, the calculated and experimental spectral patterns are also similar. As happened for the natural derivative, the higher intensity band is calculated for the ammonium vibrations, which are overlapped with the solvent absorptions in the experimental spectra.

Conclusions

In the present article, we have studied structural and vibrational properties of histamine monocation in aqueous solution. For this purpose, Fourier transform vibrational spectroscopies (infrared and Raman) and a continuum model with the hybrid three-parameter density functional B3PW91 have been used. Solvent effects have been incorporated by means of an ellipsoidal cavity model with a multipolar expansion (up to six order) of the solute's electrostatic potential. Calculations have been always performed at the 6-31+G* ab initio level. Experimental vibrational data from solutions in water and deuterium oxide have been achieved. Discussion was focused on the trans N^{τ}−H conformer of histamine monocation, which has been demonstrated as the predominant conformer in water solution. The optimized structural parameters for solved histamine monocation are near those reported for this species in the solid state by diffraction techniques, where the only conformer present is the trans N^{τ}−H. Differences come from the fact that solvation gives rise to a more uniform environment than that exists in the crystal. As an outstanding result, the calculated electronic charge localized on the imidazole ring is $^1/_3$ of the

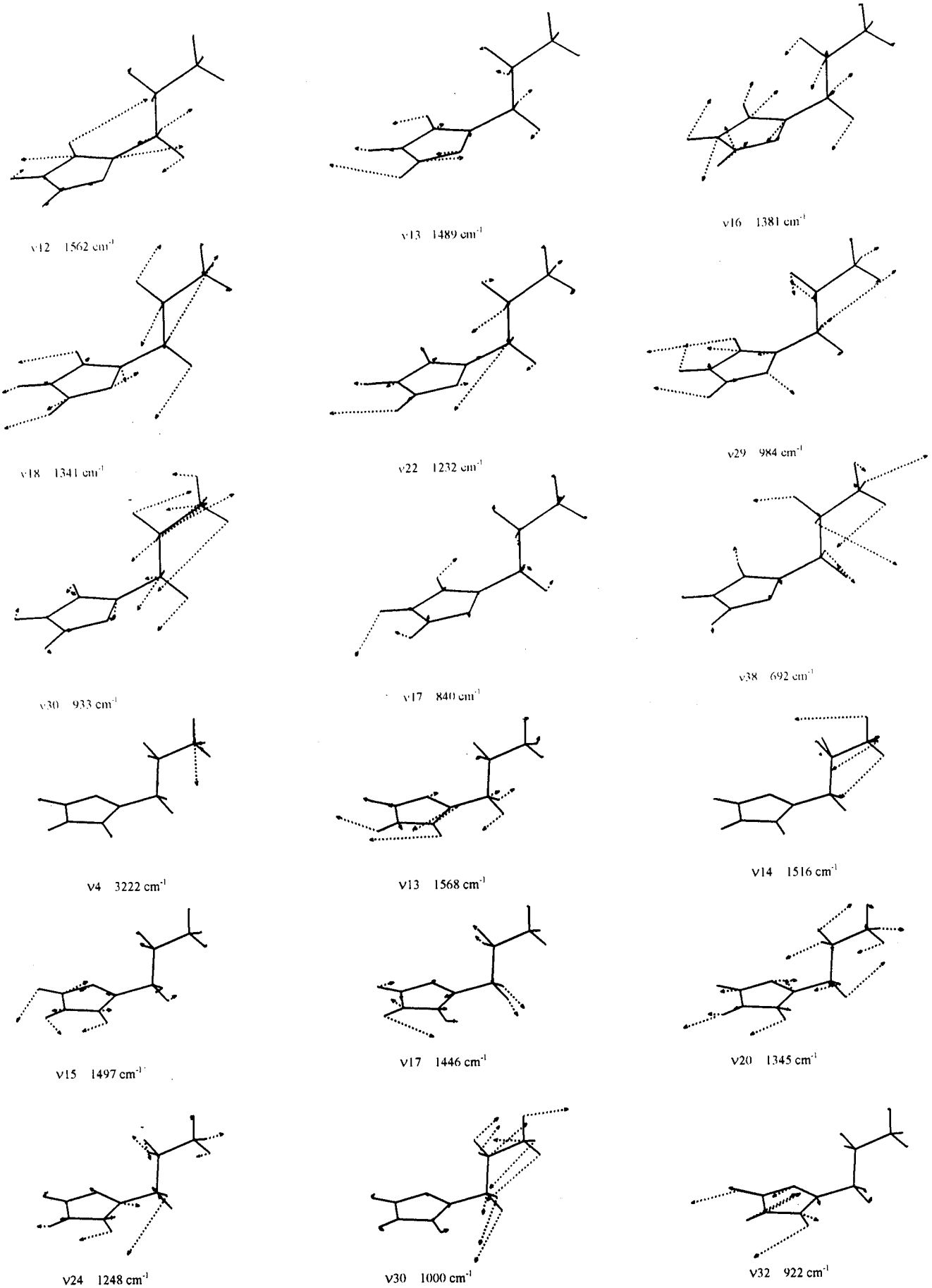

Figure 6. Atomic displacements for a selection of calculated vibrational fundamentals of natural histamine monocation and its N-deuterated derivative in aqueous solution.

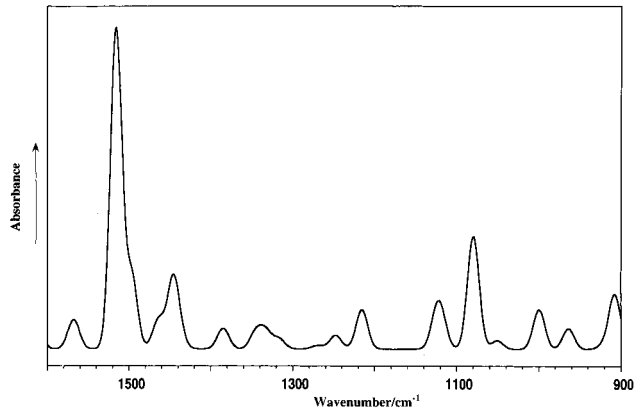

Figure 7. Theoretical SCRF/6-31+G* infrared spectrum of histamine monocation between 1600 and 900 cm^{-1}.

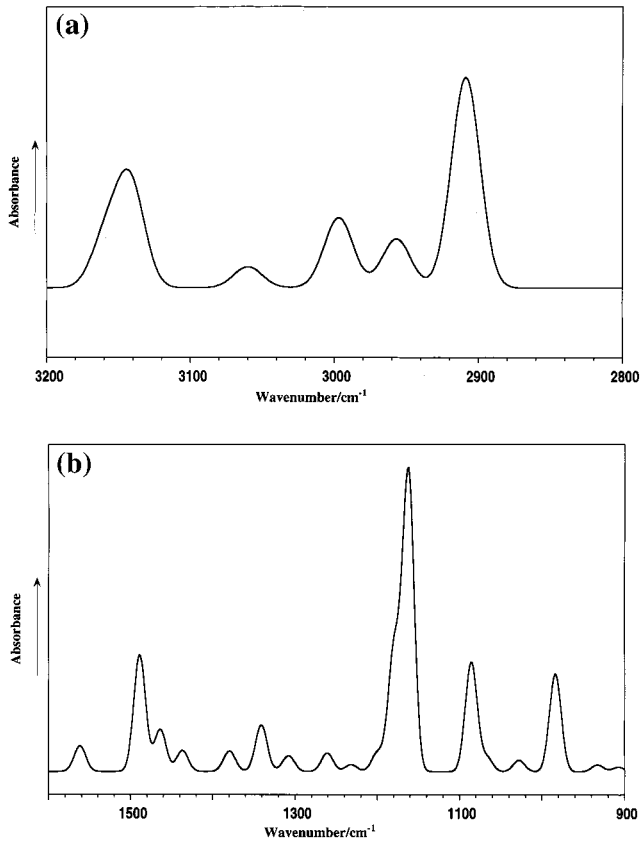

Figure 8. Theoretical SCRF/6-31+G* infrared spectrum of N-deuterated histamine monocation: (a) 3200−2800 cm^{-1} region; (b) 1600−900 cm^{-1} region.

total ionic charge, and it is close to the calculated charge for histamine free base, thus indicating similar electronic properties for both species.

A general assignment was proposed for the infrared and Raman spectra of histamine monocation in solution, based on the isotopic shifts and a previous vibrational study in solid state. Some facts can be pointed out. (i) The spectra do not show band multiplicity originated by the conformational equilibria, so that we assume the absorptions correspond to the selected structure, as the predominant. (ii) Imidazole ring stretching vibrations shift upward by 5−15 cm^{-1} upon deuteration, with the exception of the band at 1465 cm^{-1}, which shifts by −55 cm^{-1}; this evidences nonvanished amplitudes of the acidic hydrogens for the related vibrations. (iii) No band has been found to assign the δ(NH) mode; taking into account the previous point, it has to be largely distributed by the imidazole ring stretching vibrations.

Force field and normal coordinate calculations were computed to support the assignments based on experimental data. The ab initio force constants were transformed into a set of locally symmetrized internal coordinates and subsequently scaled to the experimental frequencies by using one specific and two generic scaling factors, all the them greater than 0.9. The comparison in terms of vibrational frequencies and normal coordinate descriptions has supported the most of proposed assignments. Moreover, the isotopic shifts have been correctly predicted, despite the fact they are widely distributed among the fundamentals. We have also depicted the theoretical infrared spectra for the two isotopomers on the basis of the ab initio intensities, showing a good correlation with the experimental spectra. These results evidence that solute−solvent interactions must be explicitily taking into account in order to understand the vibrational behavior of polar species in solution; in addition, the use of multipolar expansions for the interaction electrostatic potential and a cavity adapted to the molecular shape improve significantly the performance of the solvation model.

Acknowledgment. This work was partially supported by the Junta de Andalucía (Spain), research group FQM159. I.T. and E.S. thank the Spanish Ministery of Education for the research Project PB96-0792.

References and Notes

(1) Reite, O. B. *Physiol. Rev.* **1972**, *52*, 778.
(2) Pegg, A. E. *Cancer Res.* **1988**, *759*, 48.
(3) Green, J. P. *Handb. Neurochem.* **1970**, *4*, 221.
(4) Hess, H. J. *Annu. Rep. Med. Chem.* **1968**, *56*.
(5) Cooper, D. G.; Young, R. C.; Durant, G. J.; Ganellin, C. R. In *Comprenhensive Medicinal Chemistry*; Jammes, P. G., Taylor, J. B., Eds.; Pergamon Press: Oxford, 1990; Vol.3.
(6) Feuerstein, B. G.; Williams, L. D.; Basu, H. S.; Manton, L. J. *Proc. Natl. Acad. Sci. U.S.A.* **1986**, *83*, 5948.
(7) Schmid, N.; Behr, J. P. *Biochemistry* **1991**, *30*, 4357.
(8) Casero, R. A., Jr., Ed. *Biological and Therapeutic Implications of the Effects of Polyamines on Chromatin Condensation*; R. G. Landes: Austin, TX, 1995.
(9) Thomas, T. J.; Thomas, T. *Biochem. J.* **1994**, *298*, 485.
(10) Thomas, T. J.; Ashley, C.; Thomas, T.; Shirahata, A.; Sigal, L. H.; Lee, J. S. *Biochem. Cell Biol.* **1997**, *75*, 207.
(11) Schrader, B., Ed.; Infrared and Raman Spectroscopy. VCH: New York, 1995.
(12) Thomas, G. S., Ed.; Raman spectra on the conformations of biological macromolecules. *Biological Applications of Raman spectroscopy*; John Wiley and Sons: New York, 1987; Vol. 1.
(13) Clark, R. J. H., Hester, R. E., Eds.; *Advances in Infrared and Raman Spectroscopy*; Heyden: London, 1983.
(14) Duchesne, J., Ed.; *Physicochemical Properties of Nucleic Acids*; Academic Press: New York, 1973.
(15) Seuvre, A. M.; Mathlouthi, M. *Carbohydr. Res.* **1987**, *169*, 83.
(16) Ghomi, M.; Letellier, R.; Liquier, J.; Taillandier, E. *Int. J. Biochem.* **1990**, *22*, 691.
(17) Taillandier, E.; Liquier, J. *Methods Enzimol.* **1992**, *211*, 307.
(18) Bellocq, A. M.; Garrigou-Lagrange, C. *J. Chim. Phys. Physicochim. Biol.* **1970**, *64*, 1544.
(19) Itabashi, M.; Shoji, K.; Itoh, K. *Inorg. Chem.* **1982**, *21*, 3484.
(20) Davis, K. L.; McGlashen, M. L.; Morris, M. D. *Longmuir* **1992**, *8*, 1654.
(21) Collado, J. A.; Ramírez, F. J. *J. Raman Spectrosc.* **1999**, *30*, 391.
(22) Teeter, M. M. *Annu. Rev. Biophys. Chem.* **1991**, *20*, 577.
(23) Marlow, G. E.; Perkyns, J. S.; Pettitt, M. B. *Chem. Rev.* **1993**, *93*, 2503.
(24) (a) Tomasi, J.; Persico, M. *Chem. Rev.* **1994**, *94*, 2027. (b) Rivail, J. L.; Rinaldi, D. In *Computational Chemistry, Review of Current Trends*; Leszczynski, J., Ed.; World Scientific: New York, 1995. (c) Cramer, C. J.; Truhlar, D. G. In *Reviews in Computational Chemistry*; Lipkowitz, K. B., Boyd, D. B., Eds.; VCH: New York, 1996; Vol. 6.
(25) Tortonda, F. R.; Pascual-Ahuir, J. L.; Silla, E.; Tuñón, I. *Chem. Phys. Lett.* **1996**, *260*, 21.
(26) Ding, Y.; Krogh-Jespersen, K. *J. Comput. Chem.* **1996**, *17*, 338.

(27) Parr, R. G.; Yang, W. *Density Functional Theory of Atoms and Molecules*; Oxford University Press: New York, 1989.
(28) Rauhut, G.; Pulay, P. *J. Physiol. (London)* **1996**, *100*, 3093.
(29) Paiva, T. B.; Tominaga, M.; Paiva, A. C. M. *J. Med. Chem.* **1970**, *1*, 689.
(30) Rinaldi, D.; Rivail, J. L. *Theor. Chim. Acta* **1973**, *32*, 57.
(31) Rivail, J. L.; Rinaldi, D. *Chem. Phys.* **1976**, *18*, 233.
(32) Rivail, J. L.; Rinaldi, D.; Ruiz-López, M. F. In *Theoretical and Computational Models for Organic Chemistry*; Formosinho, S. J., Arnaut, L., Csizmadia, I., Eds.; Kluwer: Dodrecht, 1991.
(33) Bertrán, J.; Ruiz-López, M. F.; Rinaldi, D.; Rivail, J. L. *Theor. Chim. Acta* **1992**, *84*, 181.
(34) Rinaldi, D.; Rivail, J. L.; Rguini, N. *J. Comput. Chem.* **1992**, *13*, 675.
(35) Peng, C.; Ayala, P. Y.; Schlegel, H. B.; Frish, M. J. *J. Comput. Chem.* **1996**, *17*, 49.
(36) Assfeld, X.; Rinaldi, D. In *AIP Conference Proceedings*, *ECCC 1*; Bernardi, F., Rivail, J. L., Eds.; AIP Press: Woodbury, NY; p 59.
(37) (a) Becke, A. D. *Phys. Rev. A* **1988**, *38*, 3098. (b) Perdew, J. P.; Wang, Y. *Phys. Rev. B* **1992**, *45*, 13244.
(38) (a) Hriharan, P. C.; Pople, J. A. *Theor. Chim. Acta* **1973**, *28*, 213. (b) Clark, T.; Chandrasekhar, J.; Spitznagel, G. W.; Schleyer, P. v. R. *J. Comput. Chem.* **1983**, *4*, 294.
(39) Wong, M. W.; Frisch, M. J.; Wiberg, K. B. *J. Am. Chem. Soc.* **1992**, *114*, 52.
(40) Tortonda, F. R.; Pascual-Ahuir, J. L.; Silla, E.; Tuñon, I.; Ramírez, F. J. *J. Chem. Phys.* **1998**, *109*, 592.
(41) Frisch, M. J.; Trucks, G. W.; Schlegel, H. B.; Gill, P. M. W.; Johnson, B. G.; Robb, M. A.; Cheeseman, J. R.; Keith, T.; Petersson, G. A.; Montgomery, J. A.; Raghavachari, K.; Al-Laham, M. A.; Zakrzewski, V. G.; Ortiz, J. V.; Foresman, J. B.; Cioslowski, J.; Stefanov, B. B.; Nanayakkara, A.; Challacombe, M.; Peng, C. Y.; Ayala, P. Y.; Chen, W.; Wong, M. W.; Andres, J. L.; Reploge, E. S.; Gomperts, R.; Martin, R. L.; Fox, D. J.; Binkley, J. S.; Defrees, D. J.; Baker, J.; Stewart, J. P.; Head-Gordon, M.; Gonzalez, C.; Pople, J. A. *Gaussian 94*, revision D.3; Gaussian, Inc.: Pittsburgh, PA, 1995.
(42) Rinaldi, D.; Pappalardo, R. R. *SCRFPAC*; QCPE Indiana University: Bloomington, IN, 1992; Program number 622.
(43) Hickling, S. J.; Wooleey, R. G. *Chem. Phys. Lett.* **1990**, *166*, 43.
(44) Pulay, P.; Fogarasi, G.; Pang, F.; Boggs, J. E. *J. Am. Chem. Soc.* **1979**, *101*, 2550.
(45) Wilson, E. B. *J. Chem. Phys.* **1939**, *7*, 1047.
(46) Ganellin, C. R. *J. Pharm. Pharmacol.* **1973**, *25*, 787.
(47) Ganellin, C. R.; Pepper, E. S.; Port, G. N. J.; Richards, W. G. *J. Med. Chem.* **1973**, *16*, 610.
(48) Ganellin, C. R.; Port, G. N. J.; Richards, W. G. *J. Med. Chem.* **1973**, *16*, 616.
(49) Ganellin, C. R. *J. Med. Chem.* **1973**, *16*, 620.
(50) Farnell, L.; Richards, W. G.; Ganellin, C. R. *J. Med. Chem.* **1975**, *18*, 662.
(51) Farnell, L.; Richards, W. G.; Ganellin, C. R. *J. Theor. Biol.* **1974**, *43*, 389.
(52) Richards, W. G.; Wallis, J.; Ganellin, C. R. *Eur. J. Med. Chem.* **1979**, *14*, 9.
(53) Prout, K.; Critchley, S. R.; Ganellin, C. R. *Acta Crystallogr.* **1974**, *B30*, 2884.
(54) Worth, G. A.; Richards, W. G. *J. Am. Chem. Soc.* **1994**, *116*, 239.
(55) Hernández-Laguna, A.; Smeyers, Y. G. In *Trends in Applied Theoretical Chemistry*; Montero, L. A., Smeyers, Y. G., Eds.; Kluwer: Dordrecht, 1992.
(56) Hernández-Laguna, A.; Abboud, J. L. M.; Notario, R.; Homan, H.; Smeyers, Y. G. *J. Am. Chem. Soc.* **1993**, *115*, 1450.
(57) Hernández-Laguna, A.; Cruz-Rodríguez, Z.; Smeyers, Y. G.; Arteca, G. A.; Abboud, J. L. M.; Tapia, O. *J. Mol. Struct. (THEOCHEM)* **1995**, *335*, 77.
(58) Arteca, G. A.; Hernández-Laguna, A.; Rández, J. J.; Smeyers, Y. G.; Mezey, P. *J. Comput. Chem.* **1991**, *12*, 705.
(59) Collado, J. A.; Tuñón, I.; Silla, E.; Ramírez, F. J. Unpublished results.
(60) Bellocq, A. N.; Garrigou-Lagrange, C. *J. Chim. Phys. Physicochim. Biol.* **1970**, *67*, 1544.
(61) Davis, K. L.; McGlashen, M. L.; Morris, M. D. *Langmuir* **1992**, *8*, 1654.
(62) Itabashi, M.; Shoji, K.; Itoh, K. *Inorg. Chem.* **1982**, *21*, 3484.
(63) Loeffen, P. W.; Pettifer, R. F.; Fillaux, F.; Kearley, G. J. *J. Chem. Phys.* **1995**, *103*, 8444.